Journal of Materials Chemistry A

RSC Publishing

PAPER

View Article Online
View Journal

Microwave assisted green synthesis of MgO–carbon nanotube composites as electrode material for high power and energy density supercapacitors†

Cite this: DOI: 10.1039/c3ta01608k

K. Karthikeyan,[a] S. Amaresh,[a] V. Aravindan[ab] and Y. S. Lee*[a]

In the present study, a novel attempt has been made to fabricate an asymmetric supercapacitor based on a MgO–multi-walled carbon nanotube (MWCNT) composite as the cathode and activated carbon (AC) as the anode using an organic electrolyte (1 M $LiPF_6$ in EC : DMC 1 : 1 by volume). Supercapacitance behavior is examined by cyclic voltammetry, electrochemical impedance spectroscopy and galvanostatic charge–discharge studies. The results reveal that the test cell displayed excellent capacitance performance between 0 and 3 V. The MgO–MWCNT/AC cell delivers a specific capacitance of 66 F g^{-1} at a current density of 2.2 A g^{-1}. Cycling studies show that this cell can retain 97% of its initial capacitance after 35 000 cycles. Additionally, the MgO–MWCNT/AC cell also exhibits a maximum energy density of 30 W h kg^{-1}, which is comparable to the values obtained from other supercapacitor configurations. These results encourage utilization of the MgO–MWCNT composite as a potential electrode in developing green and low cost energy storage devices with high energy and power densities as well as prolonged cycle life.

Received 21st December 2012
Accepted 28th January 2013

DOI: 10.1039/c3ta01608k

www.rsc.org/MaterialsA

1 Introduction

Recently, the development of energy storage devices for large consumer electronic devices and hybrid electric vehicles (HEV) has attracted much interest in view of energy saving and to decrease the emission of hazardous gases into the atmosphere, respectively. The electric double layer capacitors (EDLCs) are expected to play an important role as energy storage devices for HEV due to their unique properties like high power capability at short pulse times, favorable cycling performance even at high current and long calendar life.[1–3] However, the specific energy and capacitance of EDLCs is still inadequate, which restricts them from being applied for practical use, especially for HEV due to the restricted operating potential of aqueous solutions. The electrical energy (E) accumulated in such capacitors is directly proportional to the cell voltage according to the equation $E = 1/2CV^2$ where C is the capacitance (F g^{-1}) and V is the cell voltage (volt). Based on the above equation, the energy density of the capacitor can be improved in two ways: (i) increasing the operating voltage by using organic electrolytes instead of aqueous solution (~1.2 V) due to the wider operating potential, and (ii) increasing the capacitance of the system by coupling the pseudocapacitance material as the positive electrode and the EDLC component as the negative electrode in a single cell configuration (or in other words constructing the supercapacitors with two different kinds of materials which undergo either the same or different reaction mechanisms), so called asymmetric supercapacitors (ASCs).[3,4] While the ASCs in an aqueous electrolyte have been extensively studied and reported, there are only a few reports available for organic electrolytes.[5–11] With the involvement of two different storage mechanisms/or two different kinds of electrodes in ASCs, the overall energy density and working potential of the capacitor can be expected to increase.[9,10] In the case of organic electrolytes, long-term cyclability is questionable due to the poor conducting nature of the electrolyte medium due to higher viscosity and lesser mobility of charge carriers.[12] Among the EDLC materials reported, activated carbon (AC) is the most commonly studied negative electrode for ASC applications because of its inherent properties like high surface area, excellent conductivity and high chemical stability.[12–14] Indeed, the energy density of the system is still lower than the expected level, hence the concept of making composites with electrochemically active/inactive transition metal oxides was exploited.[15] It is worth mentioning that most of the transition metal oxides, hydroxides and carbonates exhibit a pseudocapacitance behavior during electrochemical reactions, for example, hydrated RuO_2, MnO_x, NiO_x, CoO_x, MoO_x, V_2O_5 and SnO_2, *etc.*[15,16] Making the composites of the said materials with carbonaceous materials results in the combined advantages of

[a]Faculty of Applied Chemical Engineering, Chonnam National University, Gwang-ju 500-757, Korea. E-mail: leeys@chonnam.ac.kr; Fax: +82 62 530 1904; Tel: +82 62 530 1904

[b]Energy Research Institute @ NTU (ERI@N), Nanyang Technological University, Research Techno Plaza, 50 Nanyang Drive, Singapore 637553, Singapore

† Electronic supplementary information (ESI) available. See DOI: 10.1039/c3ta01608k

both pseudocapacitance and electric double layer capacitance behavior.[17] In this line, we made a novel attempt to employ an electrochemically inactive material to make a composite with MWCNT to study the influence on the capacitive behavior of the composite, since carbonaceous materials are display poor performance in organic solutes during prolonged cycling either in a symmetric or asymmetric configuration.[12]

Magnesium oxide (MgO) is an excellent functional material because of its low cost and eco-friendliness, and it has been widely used for waste hazardous chemical treatment, catalysis, refractory materials, plasma display panels and superconductor applications.[18–22] Of late, MgO coating on lithium-ion battery cathodes was also carried out to improve the cyclability, especially in elevated temperature conditions.[23] Meanwhile, few studies could be found on the use of MgO composites as an anode material for lithium-ion batteries and fuel cells.[24,25] Apparently, the energy storage application of MgO is too limited due to its inactiveness originating from the large band gap (~7.8 eV). On the other hand, MgO can be effectively used as a stabilizing agent/matrix element to extend the calendar life which was confirmed by Whittingham and co-workers.[25] Therefore, we made an attempt to synthesize a multi-walled carbon nanotube (MWCNT)–MgO composite and subsequently employed it as the positive electrode material in ASCs for the first time. In the present case, MgO certainly will act as the matrix element and is expected to improve the electrochemical performance during prolonged cycling because of its electro-catalytic behavior. Enhanced electro-catalytic and photonic activity was already reported for MgO–CNT nanocomposites.[26–28] With respect to the above considerations, the prepared composite material was used as the positive electrode material in an ASC configuration (MgO–MWCNT/AC) with 1 M $LiPF_6$ in EC:DMC as the electrolyte and the electrochemical properties were systematically studied and presented. Supercapacitive performance of the cell was investigated through cyclic voltammetry and charge–discharge studies at different current densities between 0 and 3 V and is described in detail.

2 Experimental

MWCNT and AC with a surface area of 1676 and 1600 $m^2\ g^{-1}$ were received and used without any further modification. MgO–MWCNT composites were synthesized in aqueous solution using a urea assisted microwave irradiation method followed by low temperature calcination. For the preparation of the MgO–MWCNT composite, 2.5 mg of MWCNT was mixed with 1 mM of $Mg(NO_3)_2 \cdot 6H_2O$ (99%, Sigma-Aldrich, USA) and 10 mM of urea (99%, Junsei, Japan) in 60 mL of distilled water in a 250 mL flask and sonicated for 30 min. Then the resulting solution was heated in a household microwave oven (700 W, Daewoo, Korea) for 15 min. After it was cooled down to room temperature, the resulting product was filtered, washed with deionized water followed by absolute ethanol and dried at 60 °C for 10 h in an air oven. Finally, the MgO–MWCNT composite was obtained by further calcination at 350 °C for 5 h in air atmosphere.

Phase purity of the prepared sample was examined through X-ray diffraction measurements (XRD, Rint 1000, Rigaku, Japan) equipped with Cu-Kα as the radiation source (λ = 1.54056 Å). Surface morphological features of the sample were analyzed by scanning electron microscopy (FE-SEM, S4700, Hitachi, Japan) and transmission electron microscopy (TEM, TecnaiF20, Philips, Netherlands). The Brunauer–Emmett–Teller (BET) specific surface was determined using a micromeritics ASAP 2010 surface analyzer (Micromeritics, USA). The amount of carbon content in the composite was determined by thermogravimetric analysis (TGA) from ambient temperature to 500 °C at a scan rate of 5 °C min^{-1} under oxygen flow using a thermal analyzer system (STA 1640, Stanton Redcroft Inc., UK). Raman spectra of the prepared sample were recorded using a lab Raman dispersive spectrometer (Lab Ram HR 800, Horiba, Japan).

Electrochemical measurements of the individual electrodes were analyzed by means of a CR 2032 coin-cell configuration where AC or MgO–MWCNT was used as the working electrode and a lithium foil served as both the counter and reference electrode separated by a porous polypropylene film (Celgard 3401). Composites electrodes were prepared by pressing a slurry of 80% active material (AC or MgO–MWCNT), 10% Ketjen black (KB) as a conductive additive and 10% teflonized acetylene black (TAB-2) as the binder on a 200 mm^2 nickel mesh and dried at 160 °C for 4 h in a vacuum oven. 1 M $LiPF_6$ in a mixture of ethylene carbonate (EC) and dimethyl carbonate (DMC) (1 : 1 v/v, Soulbrain, Korea) was used as the electrolyte solution. The same procedure was adopted for ASCs construction with MgO–MWCNT as the cathode and AC as the anode under an optimized mass ratio of the electrode materials (based on the electrochemical performance in half-cell configurations, the anode to cathode ratio was optimized to 1 : 1.5 with a total mass loading of 7 mg (2.8 : 4.2 mg)). Cyclic voltammetry (CV) and electrochemical impedance spectroscopy (EIS) studies were performed in an electrochemical analyzer (SP-150, Bio-Logic, France). Galvanostatic charge–discharge studies were conducted between 0 and 3 V at different current densities ranging from 0.15 to 2.2 A g^{-1} using a Won-A-Tech Battery cycler (WBCS 3000, Korea). The discharge capacitance, internal resistance, energy and power densities as well as the coulombic efficiency of ASC cells were calculated according to the formulae reported elsewhere.[29–31]

3 Results and discussion

The XRD patterns of the MgO–MWCNT nanocomposite are presented in Fig. 1. The pattern showed only the characteristic peak corresponding to MgO that matched well with the previous reports.[22,25] All strong major peaks can be indexed with the face centered cubic (fcc) MgO with the $Fm\bar{3}m$ space group based on the PDF file number 11-0293 corresponding to the lattice parameter value a = 4.21 Å.[22] Furthermore, no diffraction lines corresponding to the impurities or MWCNT were observed within the recorded area which confirmed the formation of a phase pure material. The sharp and high intensity peaks of MgO–MWCNT implied that the targeted sample has good crystallinity. To confirm the nature of the carbonaceous content in the MgO–MWCNT composite, Raman analysis was recorded for the MgO–MWCNT composite and is shown in Fig. 1b. As can

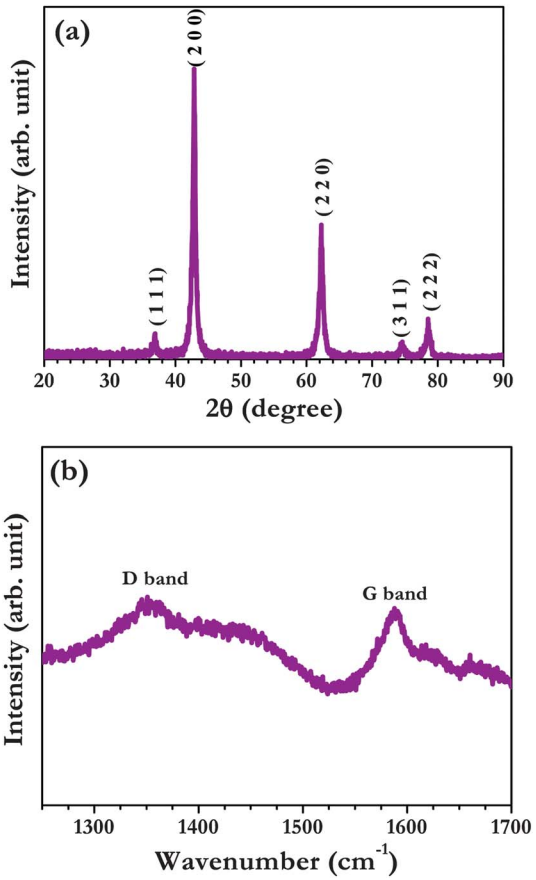

Fig. 1 (a) XRD pattern of MgO–MWCNT nanocomposite and (b) Raman spectra of MgO–MWCNT composite material prepared using the microwave irradiation method.

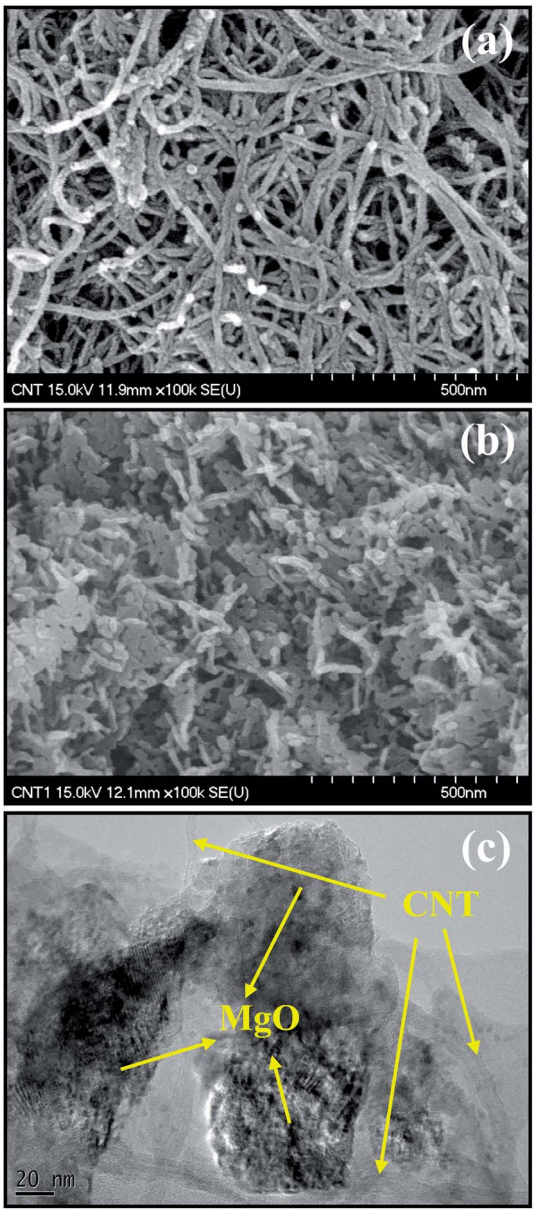

Fig. 2 SEM images of (a) MWCNT, (b) MgO–MWCNT composite materials and (c) TEM image of MgO–MWCNT nanocomposite materials.

be seen from Fig. 1b, the Raman spectra obtained for the composite material exhibited typical carbon characteristic peaks at ~1350 cm^{-1} and ~1590 cm^{-1}, which corresponds to the D and G bands, respectively.[32] The presence of the G band is related to the symmetric E_{2g} vibration mode of graphite-like materials, while the D band corresponds to the disordered carbons.[32] The intensity ratio of D and G bands (I_D/I_G) is found to be 0.95, which implies that the MgO–MWCNT composite predominantly contains sp^2 type carbon.[32] On the other hand, this considerable disorder resulted in the opening in the walls of MWCNT, which is favorable for increasing ionic/electronic transfer and hence remarkable improvement in electrochemical performance can be achieved.[33,34] The amount of carbon in the MgO–MWCNT composite was determined using TGA analysis and is presented as Fig. S1.†[34,35] The amount of carbon was calculated by the weight loss observed between 100 and 400 °C, when all the MWCNT is completely fired out, which was about 11.5 wt%.

Fig. 2 presented the SEM images of bulk MWCNT and MgO–MWCNT prepared using a urea assisted microwave irradiation method. As can be seen from Fig. 2a, the randomly entangled MWCNTs have an outer diameter of approximately 20 nm. The surface morphology of the MgO–MWCNT composite is presented in Fig. 2b. During microwave irradiation, MgO particles tend to agglomerate which forms empty spaces between particles that lacks proper conduction during the cycling process at high current rates. These void spaces between the particles were filled by MWCNT and form a network wrapping around MgO particles. This in turn provides an outstanding electronic conductivity between the MgO and MWCNT network and also makes the structure stable. It can also be seen from Fig. 2b that MWCNT was uniformly dispersed between MgO particles. Moreover, a good dispersion of the small sized MWCNT into the MgO aggregates increased the reactive sites existing for the reaction. This was further confirmed by TEM studies and the corresponding high resolution image is shown in Fig. 2c. As seen from TEM images the MgO particles were wrapped by the conductive MWCNT network. In addition, it was found that the microwave assisted synthesis of the MgO–MWCNT composite

involves small sized porous MgO particles with a narrow distribution of particle size, which uniformly attached to the surface of the MWCNT conducting network. The removal of H_2O during the annealing process made the composite materials highly porous. This porosity significantly increases its effective surface area and penetration of more electrolytes into the electrode. The former is responsible for providing more reaction sites and the latter provided a flexible structure against the mechanical stress formed during the cycling process at high current rates. It was expected that these unique properties of the composite materials would enable the achievement of excellent high rate performance. The BET surface area of MgO–MWCNT was calculated to be about ~121 $m^2\ g^{-1}$, respectively. It is well known that nanoparticles with a large surface area shorten the pathway and the large specific surface leads to the complete participation of the active material during the charge–discharge process at high current operation.

Fig. 3a shows the CV trace of MgO–MWCNT/AC cell recorded at a scan rate of 50 mV s^{-1} between 0 and 3 V. It is interesting to see from Fig. 3a and S2† that the shape of the voltammograms was near-ideal rectangular and was not distorted even at a high scan rate of 50 mV s^{-1}, indicating that the cell has a good capacitance behavior between 0 and 3 V in the presence of 1 M $LiPF_6$ in the EC:DMC electrolyte. From the CV curves, the absence of redox peaks during the anodic or cathodic sweep is apparent, which indicates the electrochemical inactiveness of MgO and is consistent with Whittingham and co-workers.[25] Hence, the role of MgO is essential to support the structural integrity to enable the stability of MWCNT electrodes during prolonged cycling. On the other hand, the storage mechanism of cells can be explained by the electrical double layer theory. Energy storage in AC electrodes is mainly based on the accumulation of ionic charge in the double layer across the electrode–electrolyte interface.[14] This clearly suggested that during the charge process PF_6^- ions are adsorbed on the surface of the MWCNT and subsequently form the double layer, whereas Li^+ ions are turbostatically adsorbed on the AC surface to balance the net charge.[14] During the discharge process, both anions and cations are desorbed from the MWCNT and AC electrodes, respectively. The cell capacitance from CV studies was calculated using the following equation $C = i/s$ where i is the current (mA) and s is the scan rate (mV s^{-1}) and the corresponding scan rate dependent capacitance is given in Fig. 3b. The maximum specific capacitance of 96 F g^{-1} was achieved from the MgO–MWCNT/AC cell at a scan rate of 1 mV s^{-1} between 0 and 3 V at ambient temperature. As can be seen from Fig. 3b, the specific capacitance of the cell linearly decreased with increase in the scan rate, which is the typical behavior of supercapacitors.[8,11] The decrease in capacitance with increasing scan rates was influenced by the surface adsorption process, which deduces the full utilization of active species for electrochemical reaction and also due to the reduction of mobility of Li-ions.[36] This pronounced capacitance value of the composite electrode could be attributed to the entanglement of MgO particles with the MWCNT conducting network that provided unobstructed pathways for Li-ion diffusion across the electrode–electrolyte interface, ensuring better contact between MgO particles and MgO/current collector. EIS study of the MgO–MWCNT/AC cell was carried out between 100 kHz and 100 mHz with ac amplitude of 10 mV in open circuit voltage conditions and is presented in Fig. 3c. The Nyquist spectra of the ASC cell consist of two main regions: a semi-circle at the high frequency region denoted as charge transfer resistance (R_{ct}) and an inclined line at approximately 45° in the low frequency region representing the diffusion control process. Based on the equivalent circuit inserted in Fig. 3c, a good fit for the experimental data was obtained as shown in the Nyquist plots. Fig. 3c clearly revealed that the R_{ct} of the MgO–MWCNT/AC cell was much lower and found to be about 9.8 Ω. Lowering the resistance enhances the reactivity of the electrode surface thereby improving the mobility of Li^+ towards the electrode and thus increasing the capacitance of the composite material.[30]

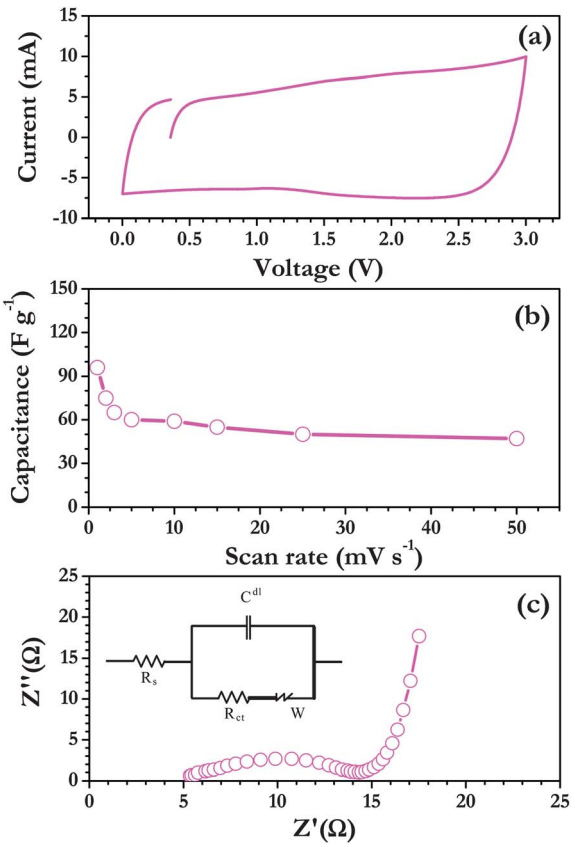

Fig. 3 (a) CV trace of MgO–MWCNT/AC cell recorded between 0 and 3 V at a scan rate of 50 mV s^{-1} with 1 M $LiPF_6$ in EC:DMC electrolyte, (b) scan rate dependent specific capacitance of MgO–MWCNT/AC cell, and (c) Nyquist plot of MgO–MWCNT/AC cell measured in open circuit voltage conditions with ac amplitude of 10 mV. The equivalent circuit for fitting is given in the inset.

Galvanostatic charge–discharge curves of the cell tested between 0 and 3 V at a current density of 0.15 A g^{-1} are presented in Fig. 4a. As seen from the charge–discharge curves, the cell potential is linearly varied with time during the cycling process. The curves also showed a linear and symmetrical feature and thereby revealed that the cells have an excellent electrochemical reversibility and capacitive characteristics in the 0–3 V range. Further, the observed traces are characteristic of EDLC behavior. The internal resistance associated with the

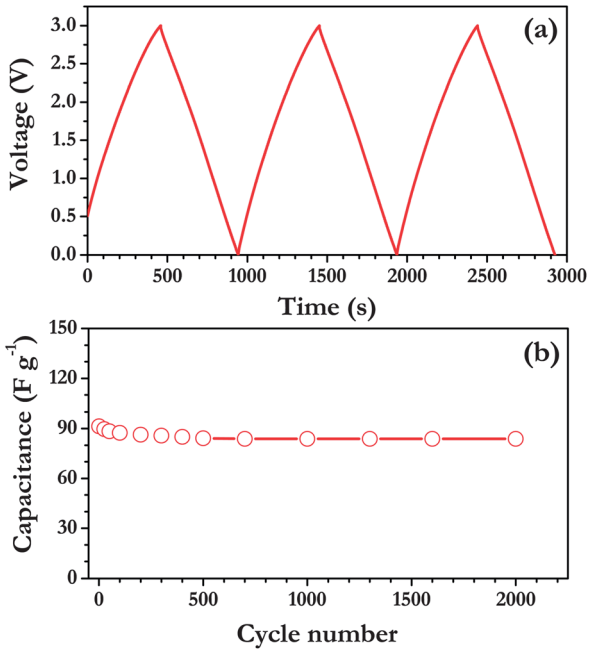

Fig. 4 (a) Typical charge–discharge curves of MgO–MWCNT/AC cell measured at a current density of 0.15 A g^{-1} between 0 and 3 V at room temperature and (b) cycling profile of MgO–MWCNT/AC cell recorded at a current density of 0.15 A g^{-1} for 2000 cycles.

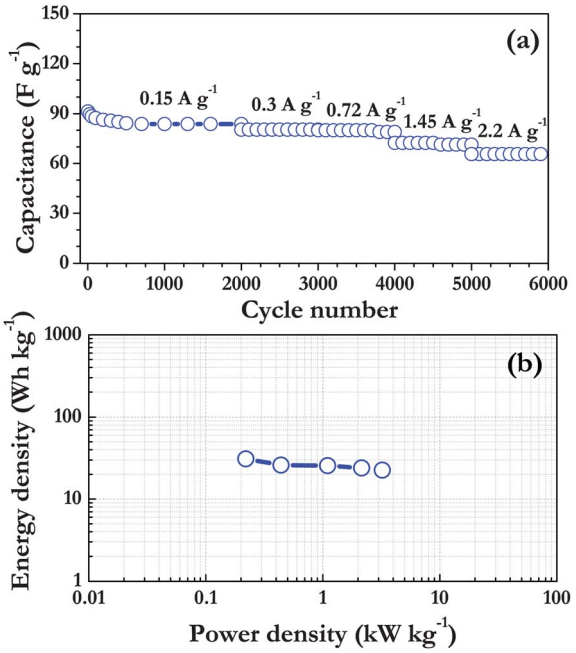

Fig. 5 (a) Rate performance of MgO–MWCNT/AC cell at different current densities from 0.15 to 2.2 A g^{-1} and (b) Ragone plot of MgO–MWCNT/AC cell.

ohmic drop (IR drop) is very low for the test cell. However, the magnitude of the IR drop increased with increasing current density (Fig. S3†). The MgO–MWCNT/AC cell delivered a specific capacitance of about 92 F g^{-1} at a current density of 0.15 A g^{-1}. It is worth mentioning that MgO nanomaterials act as catalysts to enhance the double layer formation and subsequently enhance the supercapacitive behavior. As shown in Fig. 4b, the cyclic stability of the ASC containing the MgO–MWCNT composite electrode is enhanced dramatically due to the presence of a good matrix element MgO. The MgO–MWCNT/AC cell delivered a capacitance of ~84 F g^{-1} after 2000 cycles at a current density of 0.15 A g^{-1} corresponding to a capacitance retention of ~92%.

High rate capability of the MgO–MWCNT/AC cell is presented in Fig. 5a and corresponding charge–discharge curves are presented in Fig. S3.† After cycling at a current density of 0.15 A g^{-1}, the specific capacitance faded slowly at high current rates, which may be due to the polarization effect. The MgO–MWCNT/AC ASC cell rendered excellent rate performance even at high current densities. The MgO–MWCNT/AC cell delivered specific capacitances of 80, 80, 72 and 66 F g^{-1} at current densities of 0.3, 0.72, 1.45 and 2.2 A g^{-1}, respectively. The observed values were more than 95% retention of initial values after 1000 cycles. Moreover, it is evident from the Ragone plot presented in Fig. 5b that the composite electrode is capable of delivering higher energy and power densities (both energy and power densities were calculated based on the total weight of active materials, 7 mg). For the calculation of energy density for the MgO–MWCNT/AC cell, an average potential of 1.5 V is used rather than 3 V.[8,31,34,37] The MgO–MWCNT/AC cell delivered a maximum energy density of 30 W h kg^{-1} and corresponding power density of 0.22 kW kg^{-1}. The energy density of 23 W h kg^{-1} was retained even at a power density of 3.22 kW kg^{-1}. The energy density obtained for the MgO–MWCNT/AC ASC could be compared with a graphene–MnO_2–carbon nanofibres composite,[38] TiO_2–CNT,[5] $LiTi_2(PO_4)_3$–AC,[34] ($LiMn_2O_4$ + AC)–$Li_4Ti_5O_{12}$,[39] MnO_2–AC,[6,40] V_2O_5–SWCNT[37] and AC–$Li_4Ti_5O_{12}$ (ref. 3, 41 and 42) systems comprising of similar electrolyte solutions and was higher than that of a conventional EDLC configuration.[2,3,42] Excellent electrochemical performances of the MgO–MWCNT/AC cell were ascribed to the following factors: (i) the presence of MWCNT has significantly improved the electrical conductivity and it is also involved in double layer formation, (ii) the higher specific surface area of the composite was effectively utilized for accumulation of charge carriers, (iii) uniform dispersion of the entangled MWCNTs among the pores between the MgO particles leads to a good interconnection between oxide particles at the surface and the bulk particles thereby increasing the ion/electron transport due to the electrocatalytic behavior of MgO and (iv) structural integrity provided by the MgO particles towards MWCNT during formation and depletion of the double layer during long term cyclability. Further, we believe that the porous cross-linked MgO–MWCNT nanocomposite structure was employed to store more electrolytes that avoided the electrolyte depletion during the charge–discharge as evidenced from TEM observation and hence the energy storage property of MgO–MWCNT nanocomposite was remarkably enhanced.

Apart from the high rate performance, long term cyclability is an important parameter of any energy source material to adopt in high power and energy applications. In this connection, the MgO–MWCNT/AC cell was cycled at a current density of 2.2 A g^{-1} for about 35 000 cycles. The 1st, 10 000th and 35 000th

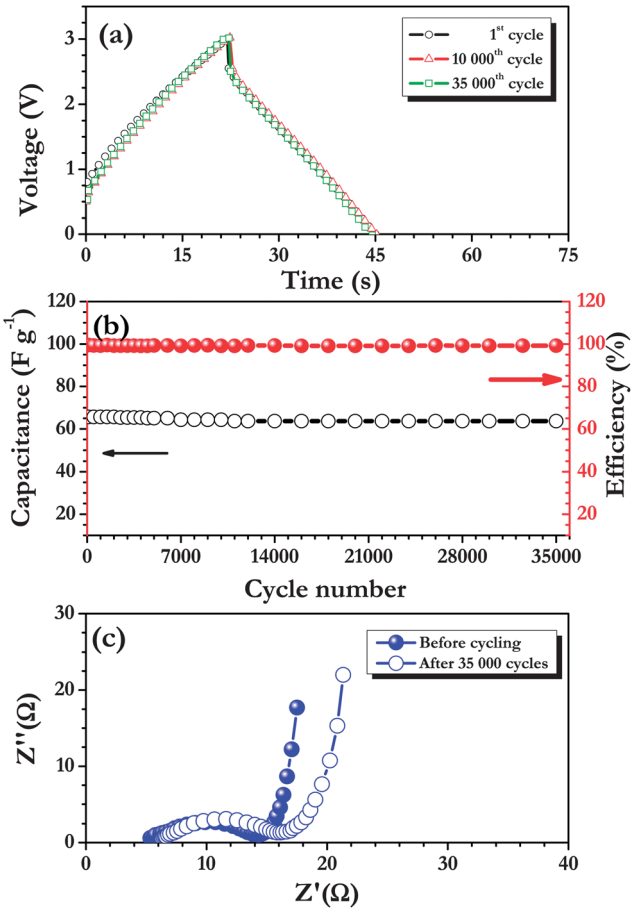

Fig. 6 (a) The 1st, 10 000th and 35 000th charge–discharge curves of MgO–MWCNT/AC cells at a current density of 2.2 A g^{-1} between 0 and 3 V, (b) plot of discharge capacitance *vs.* cycle number with coulombic efficiency and (c) Nyquist plots of MgO–MWCNT/AC cells measured before and after 35 000 cycles.

charge–discharge curves of the MgO–MWCNT/AC cell are presented in Fig. 6a. Charge–discharge curves are overlapping each other, which clearly demonstrates the excellent electrochemical reversibility and stability of the MgO–MWCNT nanocomposite. The MgO–MWCNT/AC ASC cell delivered ~66 F g^{-1} of specific discharge capacitance and retained about ~97% of its initial capacitance with more than ~99.5% of coulombic efficiency even after 35 000 cycles (Fig. 6b). Moreover, the cell also exhibited a low internal resistance of about 16 Ω. Nyquist spectra recorded before and after cycling at a current density of 2.2 A g^{-1} for 35 000 cycles and the corresponding plot are given in Fig. 6c. As can be observed from Fig. 6c, the diameter of the semi-circle was slightly larger than that before cycling, which implied that the increase in the R_{ct} value of the ASC after 35 000 cycles was very small. This outstanding cycling behavior at high current could result from the synergetic effect of intrinsic electronic and mechanical properties of MWCNTs supported by MgO.[25]

4 Conclusion

A nano-structured MgO–MWCNT composite was successfully synthesized using a microwave irradiation method. An asymmetric supercapacitor was fabricated using the prepared nano-composite as the cathode and AC as the anode in 1 M $LiPF_6$ in EC : DMC (1 : 1 by volume) solution. The cyclic voltammetric and charge–discharge studies suggested that the cell exhibited excellent capacitance behavior between 0 and 3 V at both low and high scan rates. The MgO–MWCNT/AC cell delivered maximum specific discharge capacitance, energy and power densities of 66 F g^{-1}, 23 W h kg^{-1} and 3.22 kW kg^{-1}, respectively with capacitance retention of ~97% even after 35 000 galvanostatic cycles. The enhanced performance of such supercapacitors is mainly due to the electro-catalytic activity of MgO and also provides necessary structural integrity during high current cycling. Therefore, the low cost and environmental friendly nature of MgO–MWCNT with high capacitance and energy density along with better efficiency even at high currents empowered the possibility of using them in practical applications.

Acknowledgements

This work was supported by Priority Research Centers Program through the National Research Foundation of Korea (NRF) funded by the Ministry of Education, Science and Technology (2009-0094055).

References

1 M. Winter and R. J. Brodd, *Chem. Rev.*, 2004, **104**, 4245–4270.
2 K. Naoi, W. Naoi, S. Aoyagi, J.-i. Miyamoto and T. Kamino, *Acc. Chem. Res.*, 2012, DOI: 10.1021/ar200308h.
3 K. Naoi, S. Ishimoto, J.-i. Miyamoto and W. Naoi, *Energy Environ. Sci.*, 2012, **5**, 9363–9373.
4 W. F. Mak, G. Wee, V. Aravindan, N. Gupta, S. G. Mhaisalkar and S. Madhavi, *J. Electrochem. Soc.*, 2012, **159**, A1481–A1488.
5 Q. Wang, Z. H. Wen and J. H. Li, *Adv. Funct. Mater.*, 2006, **16**, 2141–2146.
6 H. Q. Wang, Z. S. Li, Y. G. Huang, Q. Y. Li and X. Y. Wang, *J. Mater. Chem.*, 2010, **20**, 3883–3889.
7 L. Cheng, H. Q. Li and Y. Y. Xia, *J. Solid State Electrochem.*, 2006, **10**, 405–410.
8 V. Aravindan, M. V. Reddy, S. Madhavi, S. G. Mhaisalkar, G. V. Subba Rao and B. V. R. Chowdari, *J. Power Sources*, 2011, **196**, 8850–8854.
9 T. Brousse, M. Toupin and D. Belanger, *J. Electrochem. Soc.*, 2004, **151**, A614–A622.
10 M. S. Hong, S. H. Lee and S. W. Kim, *Electrochem. Solid-State Lett.*, 2002, **5**, A227–A230.
11 K. Karthikeyan, S. Amaresh, V. Aravindan, H. Kim, K. Kang and Y. Lee, *J. Mater. Chem. A*, 2013, **1**, 707.
12 P. Simon and Y. Gogotsi, *Nat. Mater.*, 2008, **7**, 845–854.
13 E. Frackowiak and F. Béguin, *Carbon*, 2001, **39**, 937–950.
14 M. Inagaki, H. Konno and O. Tanaike, *J. Power Sources*, 2010, **195**, 7880–7903.
15 D. S. Su and R. Schlögl, *ChemSusChem*, 2010, **3**, 136–168.
16 Q. Qu, S. Yang and X. Feng, *Adv. Mater.*, 2011, **23**, 5574–5580.
17 I. Plitz, A. Dupasquier, F. Badway, J. Gural, N. Pereira, A. Gmitter and G. G. Amatucci, *Appl. Phys. A*, 2006, **82**, 615–626.

18 P. Yang and C. M. Lieber, *Science*, 1996, **273**, 1836–1840.
19 A. Bhargava, J. A. Alarco, I. D. R. Mackinnon, D. Page and A. Ilyushechkin, *Mater. Lett.*, 1998, **34**, 133–142.
20 J. P. Boeuf, *J. Phys. D: Appl. Phys.*, 2003, **36**, R53.
21 R. Kakkar, P. N. Kapoor and K. J. Klabunde, *J. Phys. Chem. B*, 2004, **108**, 18140–18148.
22 S. Makhluf, R. Dror, Y. Nitzan, Y. Abramovich, R. Jelinek and A. Gedanken, *Adv. Funct. Mater.*, 2005, **15**, 1708–1715.
23 H.-J. Kweon, S. J. Kim and D. G. Park, *J. Power Sources*, 2000, **88**, 255–261.
24 Y. Shiratori, F. Tietz, H. P. Buchkremer and D. Stöver, *Solid State Ionics*, 2003, **164**, 27–33.
25 W. Zhou, S. Upreti and M. S. Whittingham, *Electrochem. Commun.*, 2011, **13**, 1102–1104.
26 B. Liu, J. H. Chen, C. H. Xiao, K. Z. Cui, L. Yang, H. L. Pang and Y. F. Kuang, *Energy Fuels*, 2007, **21**, 1365–1369.
27 Q.-C. Xu, J.-D. Lin, J. Li, X.-Z. Fu, Y. Liang and D.-W. Liao, *Catal. Commun.*, 2007, **8**, 1881–1885.
28 W. Lee, S. Im, J. Han, H. Kim, J. Yoo, K. Kim, J. Lee, J. Kim and E. Choi, *Jpn. J. Appl. Phys.*, 2002, **41**, 6550–6552.
29 K. Karthikeyan, V. Aravindan, S. B. Lee, I. C. Jang, H. H. Lim, G. J. Park, M. Yoshio and Y. S. Lee, *J. Power Sources*, 2010, **195**, 3761–3764.
30 Y. Zhu, S. Murali, M. D. Stoller, K. J. Ganesh, W. Cai, P. J. Ferreira, A. Pirkle, R. M. Wallace, K. A. Cychosz, M. Thommes, D. Su, E. A. Stach and R. S. Ruoff, *Science*, 2011, **332**, 1537–1541.
31 V. Aravindan, W. Chuiling and S. Madhavi, *J. Mater. Chem.*, 2012, **22**, 16026–16031.
32 A. C. Ferrari and J. Robertson, *Phys. Rev. B: Condens. Matter Mater. Phys.*, 2000, **61**, 14095.
33 T. Muraliganth, A. Vadivel Murugan and A. Manthiram, *Chem. Commun.*, 2009, 7360–7362.
34 V. Aravindan, W. Chuiling, M. V. Reddy, G. V. S. Rao, B. V. R. Chowdari and S. Madhavi, *Phys. Chem. Chem. Phys.*, 2012, **14**, 5808–5814.
35 B. L. Cushing and J. B. Goodenough, *Solid State Sci.*, 2002, **4**, 1487–1493.
36 K. Karthikeyan, S. Amaresh, D. Kalpana, R. Kalai Selvan and Y. S. Lee, *J. Phys. Chem. Solids*, 2012, **73**, 363–367.
37 V. Aravindan, Y. L. Cheah, W. F. Mak, G. Wee, B. V. R. Chowdari and S. Madhavi, *ChemPlusChem*, 2012, **77**, 570–575.
38 Z. Fan, J. Yan, T. Wei, L. Zhi, G. Ning, T. Li and F. Wei, *Adv. Funct. Mater.*, 2011, **21**, 2366–2375.
39 X. Hu, Z. Deng, J. Suo and Z. Pan, *J. Power Sources*, 2009, **187**, 635–639.
40 V. Aravindan, M. Reddy, S. Madhavi, G. Rao and B. Chowdari, *Nanosci. Nanotechnol. Lett.*, 2012, **4**, 724–728.
41 K. Naoi, S. Ishimoto, Y. Isobe and S. Aoyagi, *J. Power Sources*, 2010, **195**, 6250–6254.
42 K. Naoi and P. Simon, *Electrochem. Soc. Interface*, 2008, **17**, 34–37.